Electronic Supplementary Information

for

Mesoporous Gold-Silver Alloy Films towards Amplification-Free Ultra-Sensitive microRNA Detection

Materials and Reagents. Unless otherwise stated, the reagents and chemicals used in this work were of analytical grade. Potassium ferrocyanide and potassium ferricyanide were purchased from Merck KGaA, German respectively. $PS_{(18000)}$-*b*-$PEO_{(7500)}$ block copolymer was obtained from Polymer Source (Canada). Phosphate buffer saline (PBS) tablets (0.01 M phosphate buffer, 0.0027 M potassium chloride and 0.137 M sodium chloride, pH 7.4 at 25 °C) were purchased from Chem-supply (Australia). Silver nitrate ($AgNO_3$), chloroauric acid ($HAuCl_4$), and epoxy glue were obtained from Sigma-Aldrich (Australia). 5x SSC buffer (saline sodium citrate)/distilled water (Invitrogen, Australia) was used throughout the experiments. Oligonucleotides were acquired from Integrated Technologies, USA and the sequences are shown in **Table S1**. All chemicals and reagents were used as received without additional purification.

Characterization. Scanning electron microscope (SEM) images were taken with a Hitachi S-4800 scanning electron microscope with an accelerating voltage of 10 kV. Wide-angle powder X-ray diffraction (XRD) patterns were obtained with a Rigaku RINT 2500X diffractometer using monochromated Cu Kα radiation (40 kV, 40 mA) at a scanning rate of 0.5° min^{-1}. The elemental chemical analysis of the bimetallic film was performed by X-ray photoelectron spectroscopy (XPS, PHI Quantera SXM, ULVAC-PHI Inc., Japan). All samples were degassed in vacuum before carrying out the measurements.

Calculation of electrochemical surface area (ECSA). The electrochemical surface area of the mesoporous Au-Ag film (prepared with Au^{3+}:Ag^{+} ratio of 50:50) was calculated using the charge associated with the reduction of oxide by integration as follows;

Charge (Q) = Area (cm^2) / scan rate (Vs^{-1})

ECSA = Q (μC) / Q_{ref} (μC cm^{-2}), where Q_{ref} = 390 μC cm^{-2} is a calibration factor for a polycrystalline gold electrode.[S1]

Magnetic isolation and purification of miRNA (miR-9-2). Target miRNA was captured by hybridizing with a capture probe followed by functionalization with biotinylated magnetic beads and magnetic isolation and heat release of miRNA. Briefly, for probe hybridization, 10 μL of the synthetic RNA was mixed with 10 μL of 10 μM biotinylated capture probes (**Table S1**). The mixture was heated at 65 °C for 2 min and placed on a thermo-mixer under stirring for 1 h at room temperature. For magnetic isolation, 10 μL of commercial streptavidin-labelled magnetic beads (Dynabeads® MyOne™ Streptavidin C1, Invitrogen, Australia) was washed with 2×B&W solution and resuspended in 10 μL of 2×B&W buffer. The resuspended dynabeads were then added to the prepared capture probe-exosomal small RNA hybrid, mixed thoroughly, and incubated on a thermo-mixer for 30 min at room temperature to allow dynabeads labelling of capture probes *via* biotin-streptavidin interactions. After the incubation and washing with a B&W solution, the miRNA-attached beads were isolated with an external magnet and resuspended in 9 μL of RNase-free water. The resuspended miRNA-hybrid mixture was heated for 2 min at 95 ^{o}C, and the bead was immediately attached with a magnet, and the supernatant containing the desired miRNA was collected. Before applying miRNA on to Au-Ag film (prepared with Au^{3+}:Ag^{+} ratio of 50:50), the miRNA was diluted two times with 5×SSC buffer.

Supporting Figures

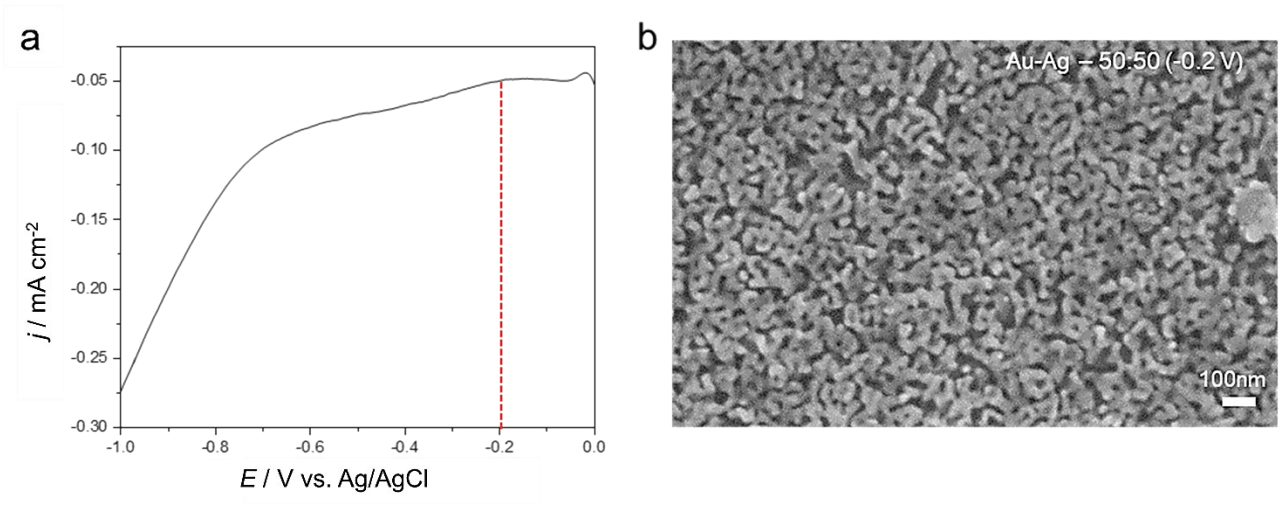

Figure S1. LSV curve obtained at a scan rate of 5 mV s^{-1} (in ice bath). (b) SEM image of the top surface of the mesoporous Au-Ag film deposited at an onset potential of -0.2 V, as determined from the LSV curve.

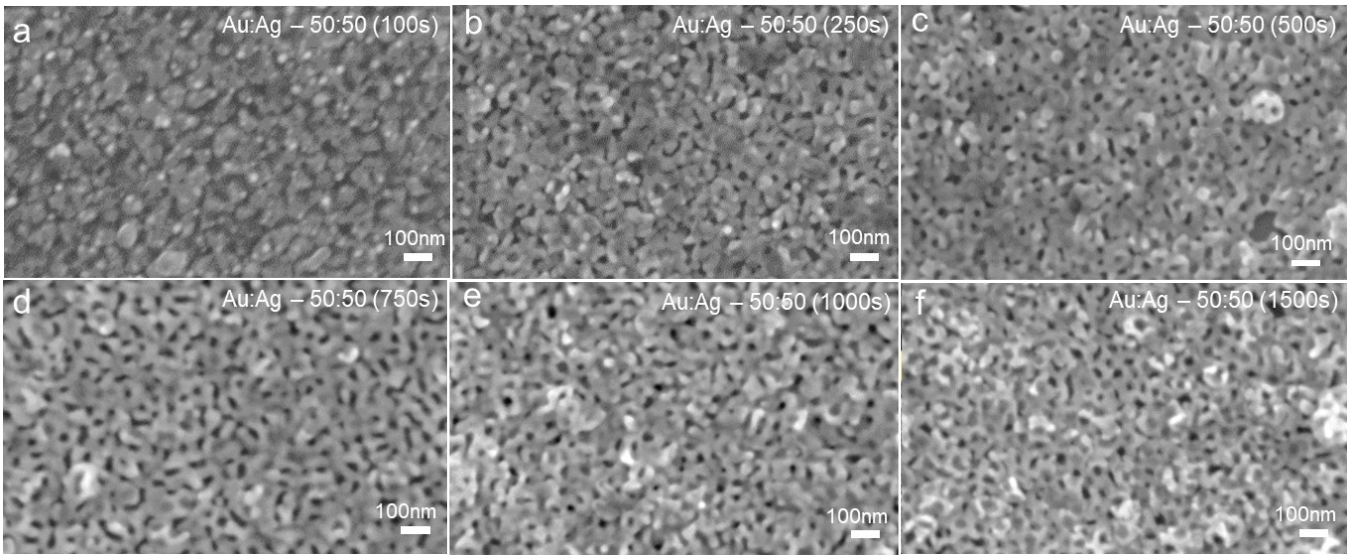

Figure S2. High-magnification SEM images of the top surfaces of the mesoporous Au-Ag films deposited for (a) 100 s, (b) 250 s, (c) 500 s, (d) 750 s, (e) 1000 s, and (f) 1500 s. The deposition potential is - 0.5 V vs. Ag/AgCl.

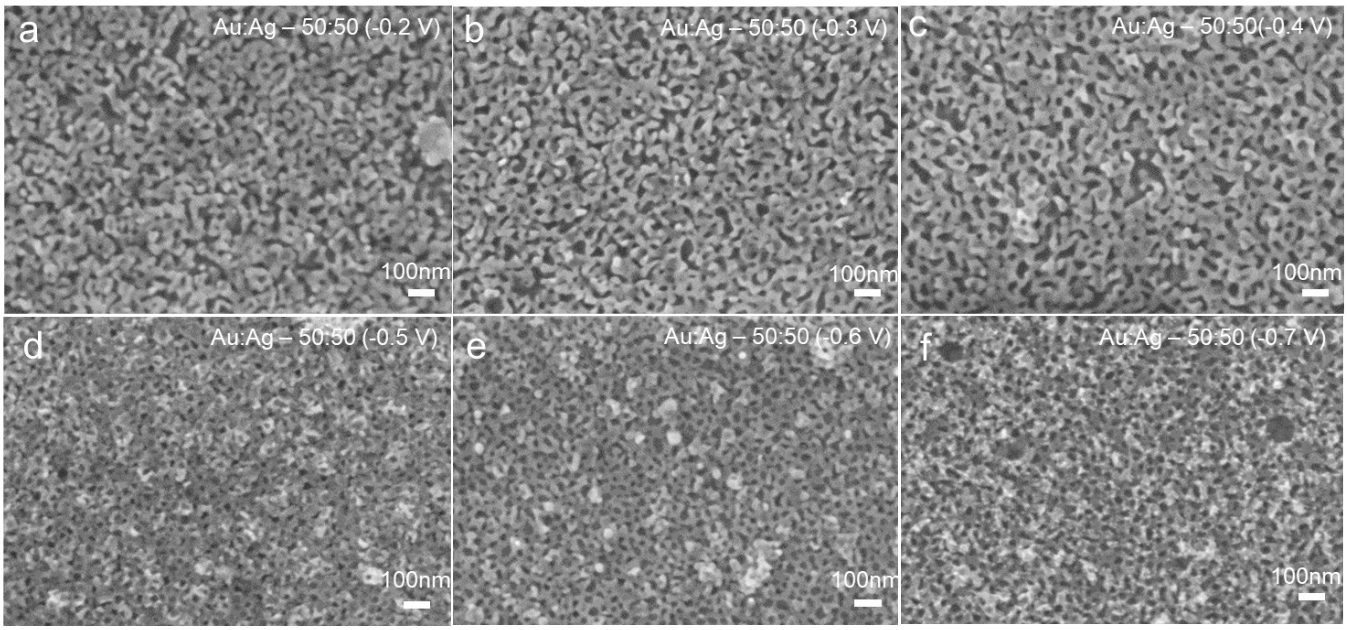

Figure S3. High-magnification SEM images of the top surfaces of the mesoporous Au-Ag films deposited at (a) -0.2 V, (b) -0.3 V, (c) -0.4 V, (d) -0.5 V, (e) -0.6 V, and (f) -0.7 V vs. Ag/AgCl.

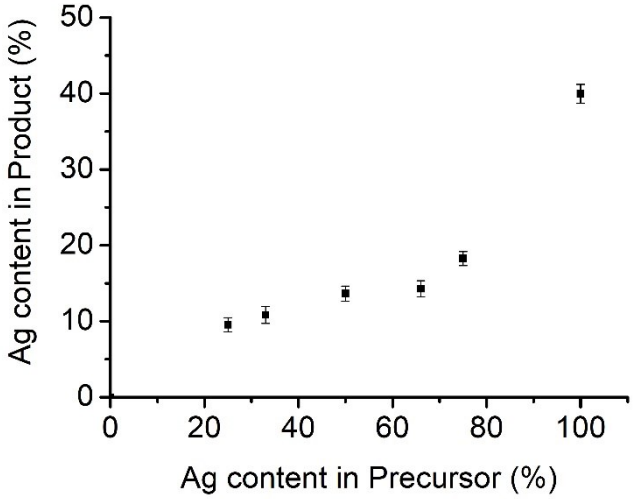

Figure S4. Relationship between the precursor composition and the product composition. The Ag content (%) in the resulting mesoporous Au-Ag films prepared with different Au-Ag precursor ratios (Au^{3+}:Ag^{+} = 0:100, 25:75, 33:66, 50:50, 66:33, 75:25 and 100:0) was measured by XPS.

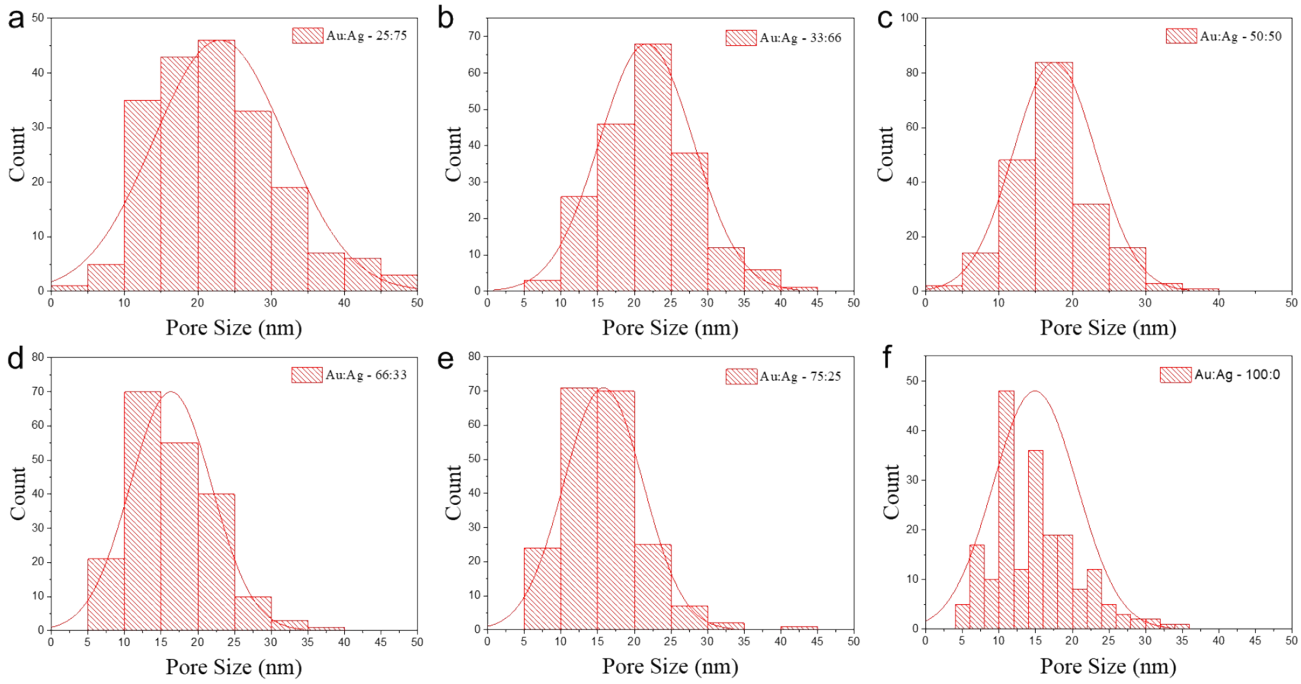

Figure S5. Pore size distribution histograms of Au-Ag and Au films prepared with Au^{3+}: Ag^{+} =25:75 (a), 33:66 (b), 50:50 (c), 66:33 (d), 75:25 (e), and 100:0 (f), respectively. The average pore sizes of Au^{3+}:Ag^{+} = 25:75, 33:66, 50:50, 66:33, 75:25, and 100:0 are 22.98 nm, 21.65 nm, 17.57 nm, 16.32 nm, 15.79 nm, and 14.9 nm, respectively.

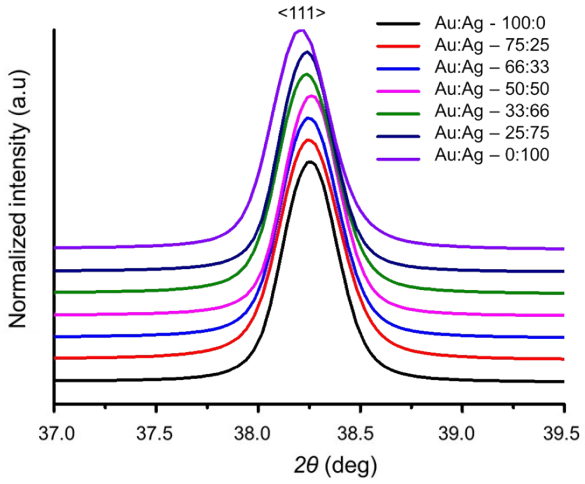

Figure S6. Wide-angle XRD patterns of Au and Au-Ag films prepared with different mole fractions of Au and Ag precursors.

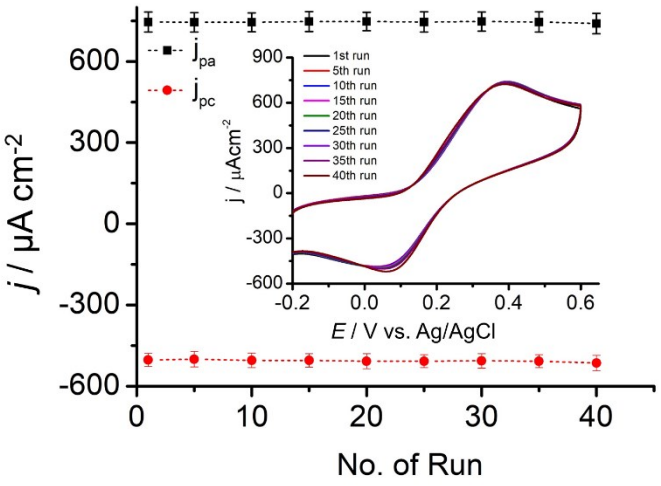

Figure S7. Stability of mesoporous Au-Ag film (prepared from Au^{3+}:Ag^{+} = 50:50) in 2 mM $[Fe(CN)_6]^{3-/4-}$ solution containing 10 mM PBS (pH 7.4). The current (Y-axis) in the figure is normalized by the geometrical substrate area (cm^2).

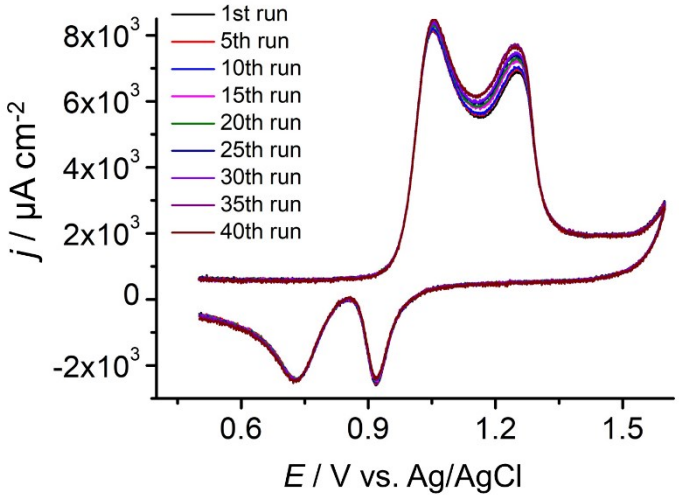

Figure S8. Stability of the mesoporous Au-Ag film (prepared with Au^{3+}:Ag^{+} = 50:50) in 0.5 M H_2SO_4 solution. The current (y-axis) in the figure is normalized by the geometrical substrate area (cm^2).

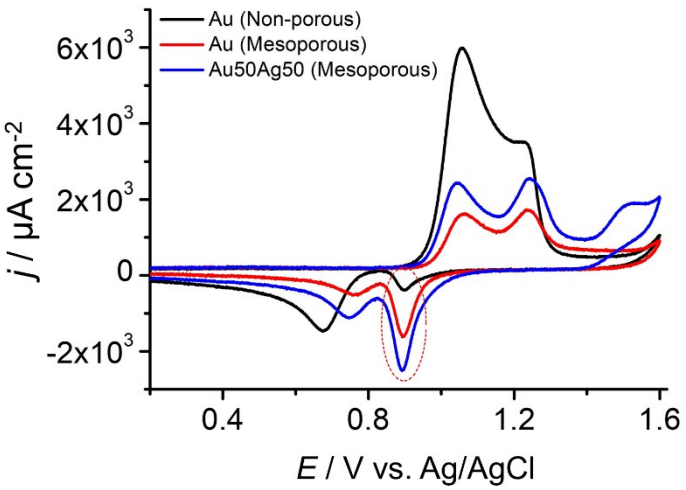

Figure S9. Cyclic voltammograms (CVs) in 0.5 M H_2SO_4 of bare Au (sputtered) substrate, mesoporous Au (prepared with Au^{3+}:Ag^{+} = 100:0) and mesoporous Au-Ag (prepared with Au^{3+}:Ag^{+} = 50:50) electrode for ECSA calculation. The current (y-axis) in the figure is normalized by the geometrical substrate area (cm^2).

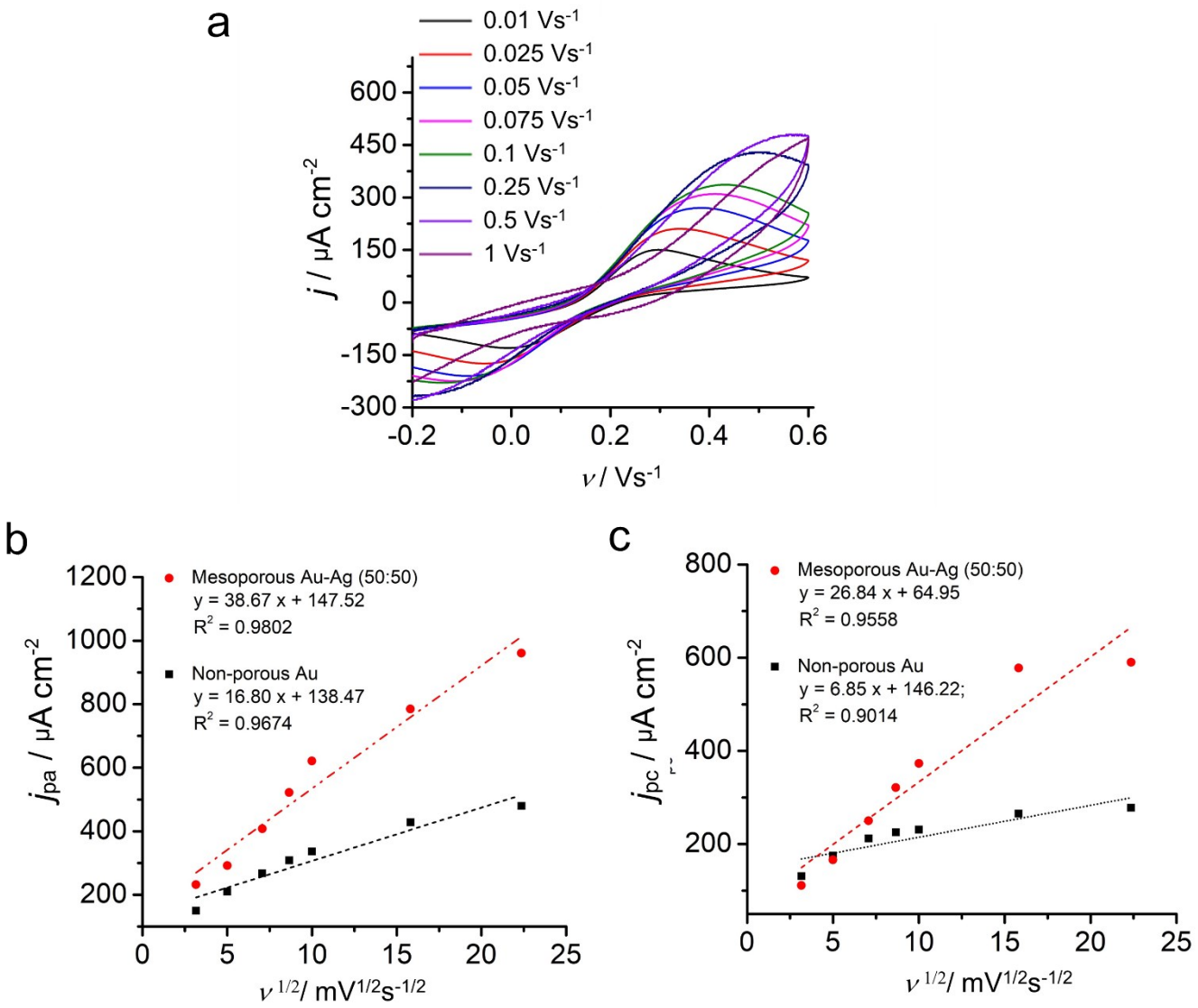

Figure 10. a) CV curves at different scan rates ranging from 0.01 to 1 mV s^{-1} for typical bare Au (sputtered) electrode in 2 mM $[Fe(CN)_6]^{3-/4-}$ solution (in 10 mM PBS). The corresponding anodic (b) and cathodic (c) redox current *versus* square root of scan rate and comparison with mesoporous Au-Ag (prepared with Au^{3+}:Ag^{+} = 50:50) film.

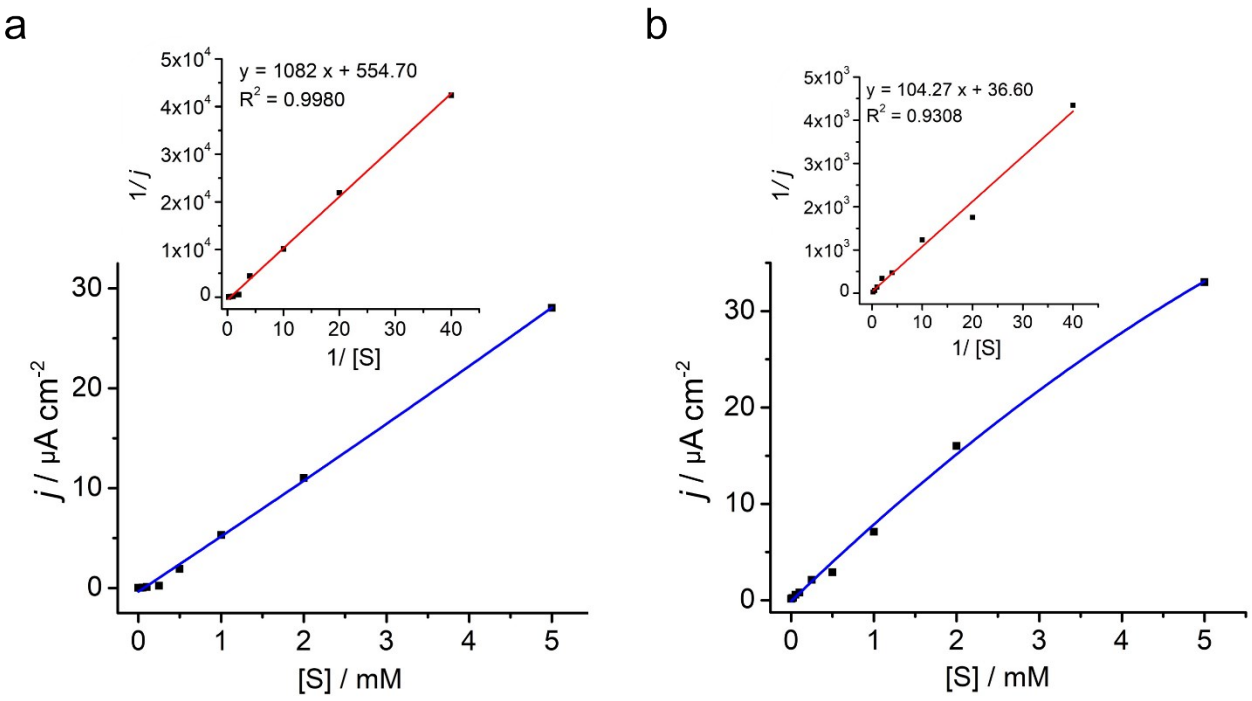

Figure S11. The calibration plot for amperometric responses of mesoporous Au100Ag0 (a) and Au0Ag100 (b) electrode with the successive addition of $[Fe(CN)_6]^{3-/4-}$ solution (10 to 1000 µM) to the 10 mM PBS buffer solution (pH-7); Inset: *the corresponding Lineweaver-Burk Model.*

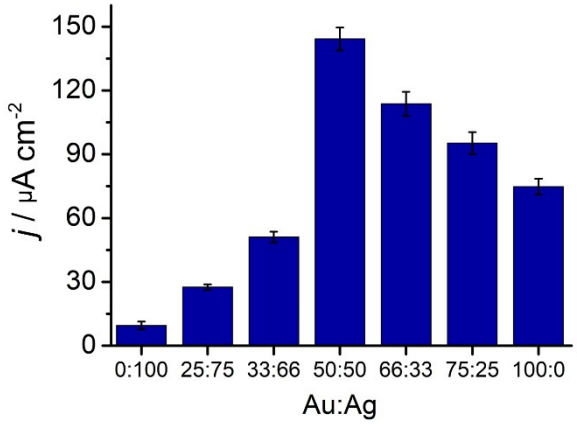

Figure S12. (a) Representation of the DPV responses (in 2 mM $[Fe(CN)_6]^{3-/4-}$ solution) after adsorption of identical amount (10 pM) of miRNA on Au-Ag electrodes with the different contents of Au and Ag.

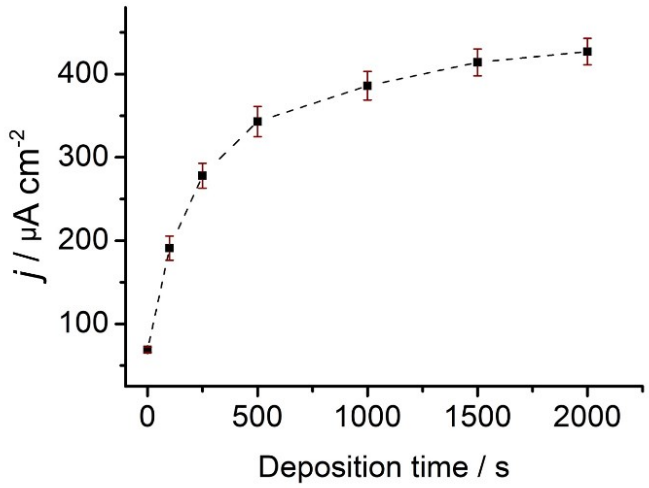

Figure S13. The miRNA detection responses of the mesoporous Au-Ag film (prepared with Au^{3+}:Ag^{+} = 50:50) electrode with different film thickness or increasing deposition time.

Supplementary Table

Table S1. Oligonucleotide sequences

Oligos	**5´-Sequences-3**
Biotinylated miR-9-2 capture Probe	TCA TAC AGC TAG ATA ACC AAA GA/3Biotin/
Synthetic miR-9-2 sequence	UCU UUG GUU AUC UAG CUG UAU GA

Table S2. Elemental compositions of Au-Ag alloys from XPS measurements

Precursor	**XPS elemental analysis**			
Ratio (Au:Ag)	Au 4f	Ag 3d	C 1s	O 1s
100:0	46.93		43.10	9.97
75:25	34.32	9.54	47.71	8.43
66:33	24.16	10.82	49.31	15.71
50:50	43.27	13.65	30.79	12.29
33:66	38.44	14.28	38.75	8.53
25:75	33.25	18.26	37.52	10.97
0:100		39.97	49.37	10.66

Table S3. XRD parameters of all the prepared samples (the average crystallite size was calculated by using Scherrer formula based on the most dominant (111) peak)

Sample	**2*θ* peak position**	**FWHM**	***d*-spacing**	**Average crystallite size (nm)**
Au	38.25508	0.33145	2.350826	25.36886427
Au25Ag75	38.2374	0.31871	2.351872	26.38153885
Au33Ag66	38.23976	0.34849	2.351733	24.12729283
Au50Ag50	38.26088	0.33042	2.350483	25.44839198
Au66Ag33	38.25179	0.34688	2.351021	24.24015896
Au75Ag25	38.25299	0.36746	2.35095	22.88264539
Ag	38.21094	0.35478	2.35344	23.6974675

Table S4. Comparative analytical performance of recent Au-Ag type sensors in which their platform employs both metals as scaffolds for microRNA detection.

Assay	Target	LOD	Comparison of LOD (approx.)	Remarks	Ref.
Electrochemical strategy on a DNA tetrahedron decorated gold electrode with AgNP-labeled signal probe	let-7a	50 aM	(100 aM *versus* 50 aM); 2 times lower	Requires isothermal rolling circle amplification	S2
Colorimetric strategy for miRNA analysis variation of silver nanoparticles (AgNPs) on gold solid interface	miR-29a-3p	1 pM	(100 aM *versus* 1 pM); 10^6 times higher	Based on hybridization chain reaction (HCR)	S3
Electrochemical detection of miRNA using *in situ* formation of Ag NPs aggregates as a label on gold NPs	miR-21	20 aM	(100 aM *versus* 20 aM); 5 times lower	Involves the covalent interaction and AgNPs aggregation as labels on the electrode surface.	S4
SERS miRNA detection through triangular Ag nanoplates (TSNPs) immobilised inside Au microcavities	miR-132-3p	10 fM	(100 aM *versus* 10 fM); 100 times higher		S5
SERS nanoprobes for multiplex detection strategy based on DNA-mediated gold−silver nanomushroom	miR-21, miR-31, miR-141	10 fM (miR-21)	(100 aM *versus* 10 fM); 100 times higher	Involves complicating SERS nanoprobe preparation	S6
SERS- assay based on Raman dye-encoded AuNPs as SERS nanotags and Ag microspheres as capture substrates	miR-21, miR-122, miR-223	2.72, 0.24, and 2.68 pM	(100 aM *versus* 2.72, 0.24, and 2.68 pM); ~3×10^4 times higher	Restricts with a limit of detection in the picomolar range and need tags.	S7
Dual colorimetric and fluorometric detection scheme based on the use of fluorescent DNA-modified silver nanoclusters (DNA-AgNCs) and gold nanoparticles (AuNPs)	miR-155	0.6 nM (colori) and 0.4 pM (fluoro)	(100 aM *versus* 0.6 nM and 0.4 pM); 4~6×10^8 times higher	It's provide semi-quantitative detetction	S8
SERS detection via electrodeposition on nano-imprinted Ag nanostructure bundles in Au nanobowls	miR-34a	50 sM	(100 aM *versus* 50 aM); 2 times lower		S9
SERS strategy via based on Ag/Au alloy shell nanoparticles	miR-21	5 fM	(100 aM *versus* 5 fM); 50 times higher	Needs duplex-specific nuclease (DSN)-assisted recycling amplification	S10

SERS detection coupled with target-catalyzed hairpin assembly based on hollow Ag/Au bimetallic nanospheres	miR-133a	0.306 fM	(100 aM *versus* 0.306 fM); 3 times higher	Involves multiple reactions and the sensitivity may be sacrificed to some extent.	S11
Chronocoulometric (CC) detetctyion of miRNA using AuNP-Fe_2O_3NC and methylene blue-ferricyanide redox cycling (MB/$[Fe(CN)_6]^{3-}$).	miR-338-3p	100 aM	(100 aM *versus* 100 aM); Same	Involves synthesis of specialized nanocubes, electrode modification and redox cycling	S12

References

S1 S. Trasatti and O. A. Petrii, *Pure Appl. Chem.,* 1991, **63**, 711-734.

S2 P. Miao, B. Wang, F. Meng, J. Yin and Y. Tang, *Bioconjug. Chem.*, 2015, **26**, 602-7.

S3 J. Miao, J. Wang, J. Guo, H. Gao, K. Han, C. Jiang and P. Miao, *Sci. Rep.*, 2016, **6**, 32219.

S4 L. Liu, Y. Chang, N. Xia, P. Peng, L. Zhang, M. Jiang, J. Zhang and L. Liu, *Biosens. Bioelectron.*, 2017, **94**, 235-242.

S5 H. McArdle, E. Spain, T. Keyes, R.L. Stallings, M. Brennan-Fournet and R.J. Forster, *Electrochem. Commun.*, 2017, **79**, 23-27.

S6 J. Su, D. Wang, L. Norbel, J. Shen, Z. Zhao, Y. Dou, T. Peng, J. Shi, S. Mathur, C. Fan and S. Song, *Anal. Chem.*, 2017, **89**, 2531-2538.

S7 W. Zhou, Y.F. Tian, B.C. Yin and B.C. Ye, *Anal. Chem.*, 2017, **89**, 6120-6128.

S8 Y. S. Borghei, M. Hosseini, M.R. Ganjali and H. Ju, *Microchim. Acta*, 2018, **185**, 286.

S9 T. Lee, J.S. Wi, A. Oh, H.K. Na, J. Lee, K. Lee, T.G. Lee and S. Haam, *Nanoscale*, 2018**, 10**, 3680-3687.

S10 D. Ma, C. Huang, J. Zheng, J. Tang, J. Li, J. Yang and R. Yang, *Biosens. Bioelectron.*, 2018**, 101**, 167-173.

S11 Y. Sun and T. Li, *Anal. Chem.*, 2018, **90**, 11614-11621.

S12 M. K. Masud, R. G. Mahmudunnabi, N. B. Aziz C. H. Stevens D. Do-Ha, S. Yang, I. P. Blair, M. S. A. Hossain, Y. B. Shim, L. Ooi, Y. Yamauchi and M. J. A. Shiddiky, *ChemElectroChem*, 2020. DOI:10.1002/celc.202000828